Princeton Plasma Physics Laboratory

PPPL- 4483

PPPL- 4483

Beam Distribution Modification By Alfven Modes

R.B. White, N. Gorelenkov, W.W. Heidbrink, and M.A. Van Zeeland

January, 2010

Prepared for the U.S. Department of Energy under Contract DE-AC02-09CH11466.

Princeton Plasma Physics Laboratory
Report Disclaimers

Full Legal Disclaimer

Trademark Disclaimer

PPPL Report Availability

Princeton Plasma Physics Laboratory:

http://www.pppl.gov/techreports.cfm

Office of Scientific and Technical Information (OSTI):

http://www.osti.gov/bridge

Related Links:

U.S. Department of Energy

Office of Scientific and Technical Information

Fusion Links

Beam distribution modification by Alfvén modes

R. B. White,[1] N. Gorelenkov,[1] W. W. Heidbrink,[2] and M.A. Van Zeeland[3]

[1]*Plasma Physics Laboratory, Princeton University,*

P.O.Box 451, Princeton, New Jersey 08543

[2]*University of California, Irvine, California, 92697*

[3]*General Atomics, P.O. Box 85608, San Diego, California, 92186-5608*

(Dated: January 8, 2010)

Abstract

Modification of a deuterium beam distribution in the presence of low amplitude Toroidal Alfvèn (TAE) eigenmodes and Reversed Shear Alfvèn (RSAE) eigenmodes in a toroidal magnetic confinement device is examined. Comparison with experimental data shows that multiple low amplitude modes can account for significant modification of high energy beam particle distributions. It is found that there is a stochastic threshold for beam transport, and that the experimental amplitudes are only slightly above this threshold. The modes produce a substantial central flattening of the beam distribution.

/Orbit0/pplas.tex

PACS numbers: 52.25.Fi, 52.25.Gj

I. INTRODUCTION

Energetic ion populations often drive Alfvén waves unstable in toroidal magnetic confinement devices [1] and similar instabilities may be driven by alpha particles or high-energy beam ions in ITER [2]. A goal of current research is to predict and control fast-ion transport in ITER and other future devices.

Deuterium beam ions in DIII-D plasmas drive many toroidicity-induced Alfvén eigenmodes (TAE) and reversed shear Alfvén eigenmodes (RSAE) unstable [3]. The mode structure is measured with electron cyclotron emission (ECE) and beam-emission spectroscopy (BES) diagnostics. Comparisons of the ECE measurements with the linear eigenfunctions calculated by the MHD code NOVA show excellent agreement in the mode shape [3] and temporal evolution [4][5]. Saturated mode amplitudes are derived by scaling the prediction of a synthetic ECE diagnostic applied to NOVA calculated eigenfunctions. The same scaling factor gives quantitative agreement with the electron density fluctuations measured by BES [3]. The resultant beam-ion transport is measured by five independent techniques [6, 7], including spatially-resolved fast-ion D-alpha (FIDA) spectroscopy. The data imply strong central flattening of the fast-ion profile during the early phase of the discharge when many Alfvén modes are unstable [6, 7]. In plasmas without appreciable MHD activity, the FIDA profiles agree well [8] with the profiles predicted by the NUBEAM module [9] of the TRANSP code but, in the presence of the strong TAE and RSAE activity, the profile in the inner half of the plasma is much flatter than classically expected [6, 7].

To test the assumption that the Alfvén modes cause the additional fast-ion transport, in previous works [6, 7], we inserted NOVA calculated eigenfunctions that were experimentally validated by ECE measurements into the guiding center code ORBIT [10] and calculated the expected fast-ion transport but found values too small to account for the profile modification. A similar approach was successfully applied to observations of fast-ion transport by fishbones in the Poloidal Divertor Experiment [11] and tearing modes in numerous toroidal devices [12–15]. There have been many previous numerical studies of fast-ion transport by Alfvén eigenmodes [16–22] but, in all cases, appreciable fast-ion transport occurred when the mode amplitude was $\delta B/B \sim 10^{-3}$. We have discovered [23] that the system possesses a stochastic threshold, and that the experimental values are only slightly above it, making simulations very sensitive to mode amplitudes and other small effects. In particular, the omission of

the electric potential associated with the magnetic perturbations, but including all observed modes and harmonics as well as the neoclassical transport through pitch angle scattering, leads to beam transport more than an order of magnitude too small to explain the observed profile flattening.

II. RESONANCE

Only through resonance with a perturbation is a significant modification of the particle distribution possible, since the mode amplitudes are known to be very small, with $\delta B/B \simeq 2 \times 10^{-4}$. We are interested in passing particle resonance. It is fairly easy to assess the effect of a particular mode on the particle distribution by examining a Poincaré plot for a particular choice of either co-moving or counter-moving particles, which we refer to as a kinetic Poincaré plot to distinguish it from a plot of the magnetic field. Points are plotted in the poloidal cross section whenever $n\zeta - \omega_n t = 2\pi k$ with k integer, where ζ is the toroidal particle coordinate, and ω_n is the mode frequency. The toroidal motion then gives successive Poincaré points, with $\Delta\zeta = \omega_t \Delta t$ satisfying

$$n\omega_t - \omega_n = 2\pi/\Delta t. \tag{1}$$

where ω_t is the toroidal transit frequency. For there to be a periodic fixed point in the poloidal angle θ with period m' we also require $\Delta\theta = 2\pi l/m'$ with l integer. But neglecting particle drift we also have $\Delta\theta = \omega_t \Delta t/q$, with q the magnetic field helicity, giving

$$[n - m'/ql]\omega_t = \omega_n, \qquad q = \frac{m'/l}{n - \omega_n/\omega_t}, \tag{2}$$

this last equation determining the location of the resonance. A resonance appears whenever there exist integers m', l such that this relation can be satisfied. Since the Alfvèn frequency is generally large, only rapidly moving particles are capable of participating, and important interaction occurs only for high energy heating particles or for fusion products such as alpha particles. Note that for co-moving passing particles ($\omega_t > 0$) and $n > 0$, increasing the mode frequency ω_n increases the q value of the resonance, and increasing energy or pitch (and thus ω_t) decreases the q value of the resonance. These islands exist in real space and in the energy variable.

However Eq. 2 was calculated neglecting the particle drift motion. In order to examine the effect of resonance for arbitrary energy and pitch, as well as in a general equilibrium we use

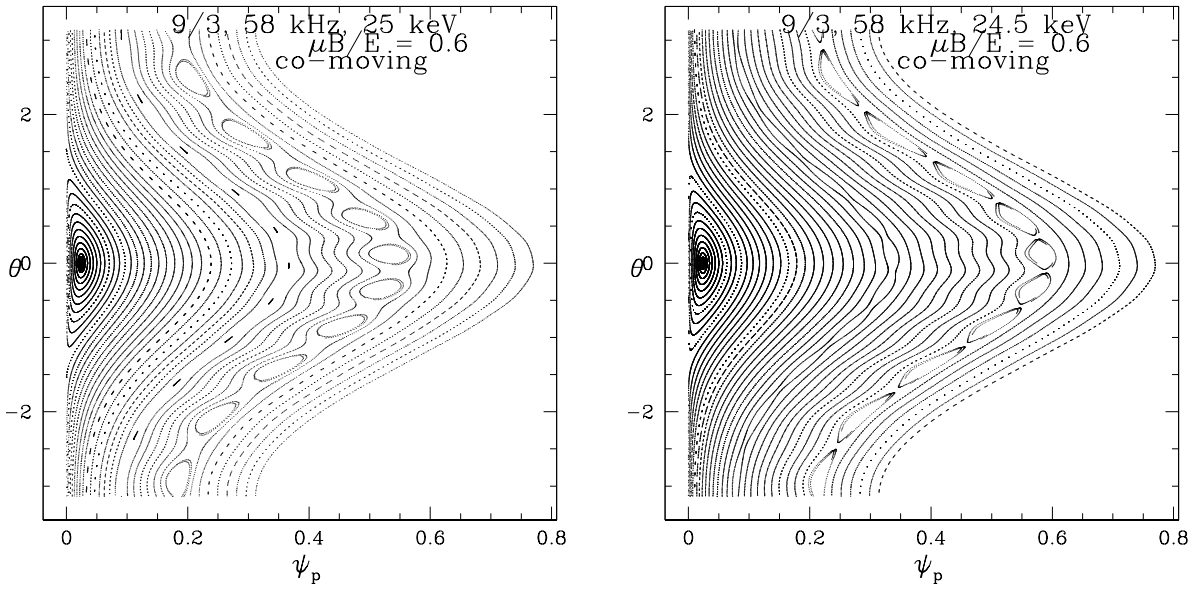

FIG. 1: Kinetic Poincaré plots for mode $m/n = 9/3$, showing energy dependence of the $m' = 10$ resonances. Shown are the resonances for a 9/3 perturbation on particles of 25 keV and 24.5 keV.

a numerical method of displaying these resonances. Energy is not conserved since the mode is time dependent, and for a mode of a single n value the perturbation of the Hamiltonian includes ζ and t only in the form $H(n\zeta - \omega_n t)$. Similarly, canonical toroidal momentum is not conserved, and from Hamilton's equations $dP_\zeta/dt = -\partial_\zeta H$, and $dE/dt = \partial_t H$ and thus for fixed n we find that $\omega_n P_\zeta - nE$ is constant in time.

To obtain a kinetic Poincaré plot the distribution must be initiated with a fixed value of μ and $\omega P_\zeta - nE = c$. This plot shows islands indicating resonance of the particles with the perturbation, and it includes all nonlinear couplings, deviation of the orbits from a single flux surface due to drift, and particle precession rates. In Fig. 1 are shown kinetic Poincaré plots for different modes in an equilibrium with the reversed shear q profile of the DIIID equilibrium studied, to illustrate the islands produced by modes with $\delta B_r/B$ of order 10^{-4}. Energies and pitch are chosen to reflect values near the peak of a DIII-D deuterium ion beam distribution, with values of $\mu B/E$ approximately equal to 0.6. The large displacement in ψ_p versus θ of approximate $cos(\theta)$ form is the drift motion of the co-injected beam. Fig. 1 demonstrates the resonance position shift of an $m' = 10$ island chain due to a change in energy, decreasing the energy increases the q value, and for this radius the surface moves outward. This resonance was produced by a single harmonic with $m = 9$, and $n = 3$.

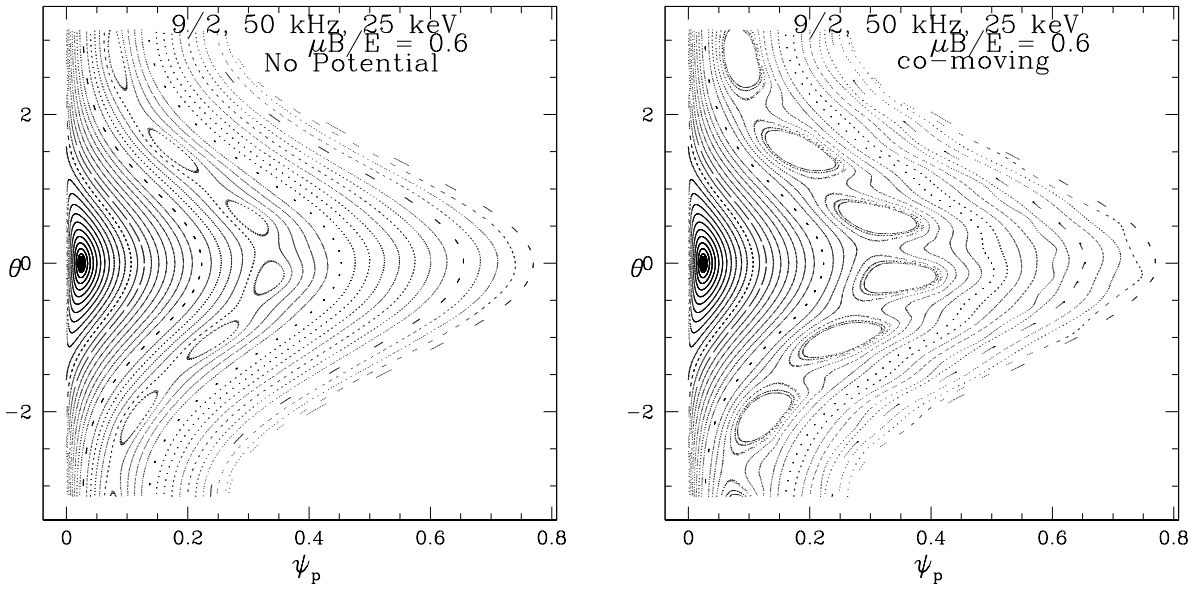

FIG. 2: Kinetic Poincaré plots for mode $m/n = 9/2$, showing the effect of the potential on 25 keV beam particles for a 50 kHz mode.

Ion motion is further modified by the fact that the rapid mobility of the electrons makes the electric field experienced by the ions parallel to the magnetic field equal to zero. Thus in general it is necessary to add an electric potential Φ to cancel the parallel electric field induced by $d\vec{B}/dt$.

In Fig. 2, are shown kinetic Poincaré plots with and without the electric potential for a 50 kHz TAE mode and 25 keV deuterium ions, giving in the DIII-D equilibrium $\omega/\omega_0 = 3\times10^{-3}$, $\rho/R = 10^{-2}$, with ω_0 the cyclotron frequency, and ρ the cyclotron radius of the particle. The effect of the potential can be neglected only for modes with $\omega/\omega_0 \ll \rho/R$. If these terms are comparable the potential can have a significant effect on island size.

III. BEAM MODIFICATION

The initial beam profile was obtained from a TRANSP calculation of the distribution function [9], with energy ranging from 20 to 80 keV. TRANSP produces a list of 10^5 to 10^6 particles characterizing the deuterium beam, giving the velocity and position of all particles at a particular time. There are beam particles present with lower energy than this, but we are interested in the effect of the modes on high energy particles only, so the distribution is

truncated at 20 keV. The energy distribution is shown in Fig. 3, along with the distributions in poloidal flux and in pitch, with the pitch expressed in terms of the magnetic moment μ and energy E. The pitch is $\lambda = v_{\|}/v = \pm\sqrt{1-\mu B/E}$, with v the velocity. The distribution is almost entirely co-passing, and significantly peaked around $\mu B_0/E = 0.6$, with B_0 the on-axis field strength. The distribution in energy has a dominant contribution at $E \simeq 25KeV$. The flux distribution simply gives the number of particles in equal size zones of poloidal flux; it is approximately proportional to the particle density.

A large spectrum of TAE and RSAE modes was observed to be present with amplitudes in the range of $\delta B/B \approx 10^{-4}$, as determined by density and temperature fluctuation measurements. The spectrum of modes we use in the simulation is given by NOVA, with the amplitudes of the various modes fixed by comparison with temperature fluctuation measurements. An example of the comparison of a NOVA calculated eigenmode with ECE data is shown in figure 4(a) for a $f = 78$ kHz TAE, where the perturbed electron temperature (δT_e) is plotted vs. the normalized square root of toroidal flux (ρ)[5]. For comparison with ECE measurements, a synthetic diagnostic as described in reference [3] was used to process the NOVA predicted temperature perturbation. The actual poloidal harmonic content/structure comprising the TAE is shown in figure 4(b), where it is seen that at least 10 harmonics contribute significantly, something typical of the global TAEs discussed here. By scaling the NOVA prediction using a single constant to match the ECE data [figure 4(a)] the amplitude of the perturbation wavefields is obtained. The inferred amplitude is shown in figure 4(c) as a function of major radius (R) along the device midplane, where the radial magnetic field perturbation (δB_r) is scaled to the local magnetic field strength B. For the majority

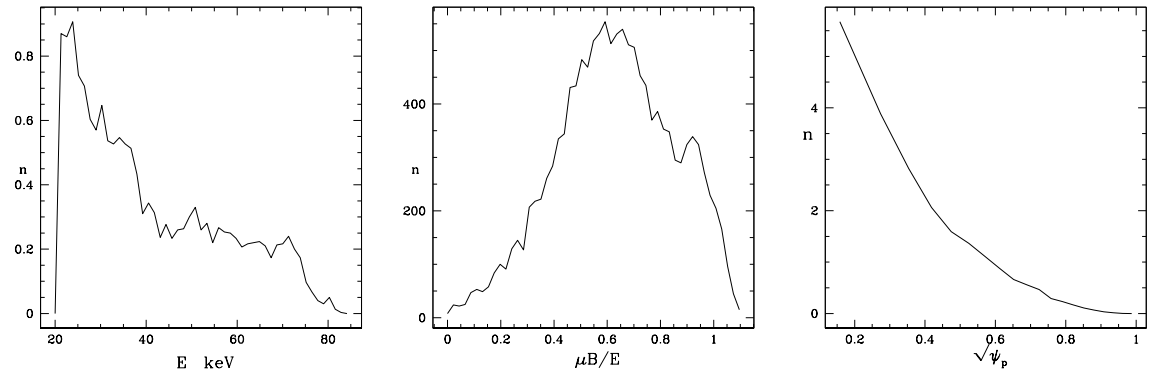

FIG. 3: Initial Beam distribution in energy, pitch, and flux surface.

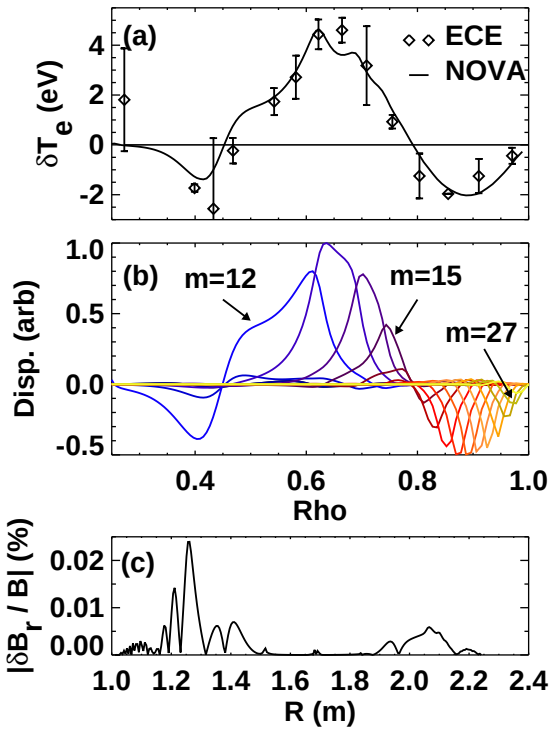

FIG. 4: (color online) (a) Synthetic ECE diagnostic prediction (solid) using NOVA calculated $f = 78$ kHz global TAE overlayed with ECE measurements (diamonds). NOVA prediction scaled by single constant to match ECE data. (b) Poloidal harmonics comprising TAE from panel (a). (c) Calculated radial component of magnetic field fluctuation along device midplane (vs. major radius) using amplitude obtained from comparison with ECE data[5].

of experiments on DIII-D, typical AE amplitudes obtained in this manner are found to be $\delta B_r/B < 10^{-3}$.

The frequency dependence of the spectrum of modes included in the simulation is shown in Fig. 5. Only the RSAE modes have significant frequency variation over the range of time considered, the TAE modes are fairly constant in frequency.

Resonance islands produce transport in two ways. If nearby islands overlap as first described by Chirikov, stochastic transport results. However, even in the absense of this, islands produce additional particle displacement from their nominal drift surface, and in the presence of collisions this gives a diffusion term with a step size given by the island width. To examine the question of chaotic transport we launch a distribution of 2000 particles all on the same drift surface, initially all with a single value of energy and pitch at the outer midplane, but distributed randomly toroidally. We choose a distribution characteristic of

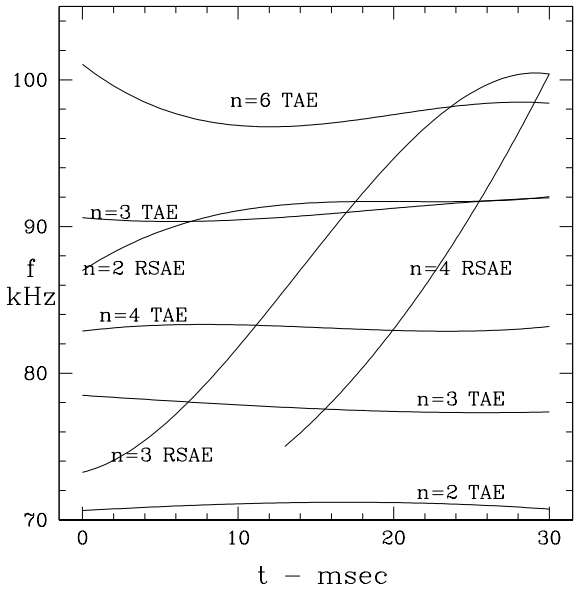

FIG. 5: Time dependence of the modes in the spectrum

the beam, with a pitch of $\lambda = 0.6$ and an energy of 25 keV. In Fig. 6 is shown the final particle positions after 7 $msec$ in the presence of the modes used in the simulation, with magnitude $dB/B \simeq 1.2 \times 10^{-4}$, (a), and $dB/B \simeq 1.6 \times 10^{-4}$, (b) but no collisions.

It is clear from this figure that the density level of the small scale islands in the simulation allows for global stochastic transport, with a stochastic threshold $1.2 \times 10^{-4} < dB/B < 1.6 \times 10^{-4}$. In the interval between these numbers there is a gradual increase in the number of particles found outside the original drift surface after 7 $msec$, but it is clear that even at $dB/B = 1.4 \times 10^{-4}$ the last KAM surface has been broken, and that a very long simulation would produce a flat distribution. Even for larger amplitudes the particle excursions are limited radially, indicating that the stochastic domain exists only in the core of the device, explaining the flattening of the beam distribution in the core, but the absence of changes further out in the distribution. Modes have significant amplitude only in the plasma core. The stochastic threshold very near the experimental amplitudes explains the failure of previous attempts to describe this profile flattening. A small reduction in the efficacy of the modes, or in the number of harmonics, moves the system below stochastic threshold, and the resulting particle redistribution is due solely to the slow collisional transport between island chains.

To test the effect of the frequency variation, runs were performed with and without the

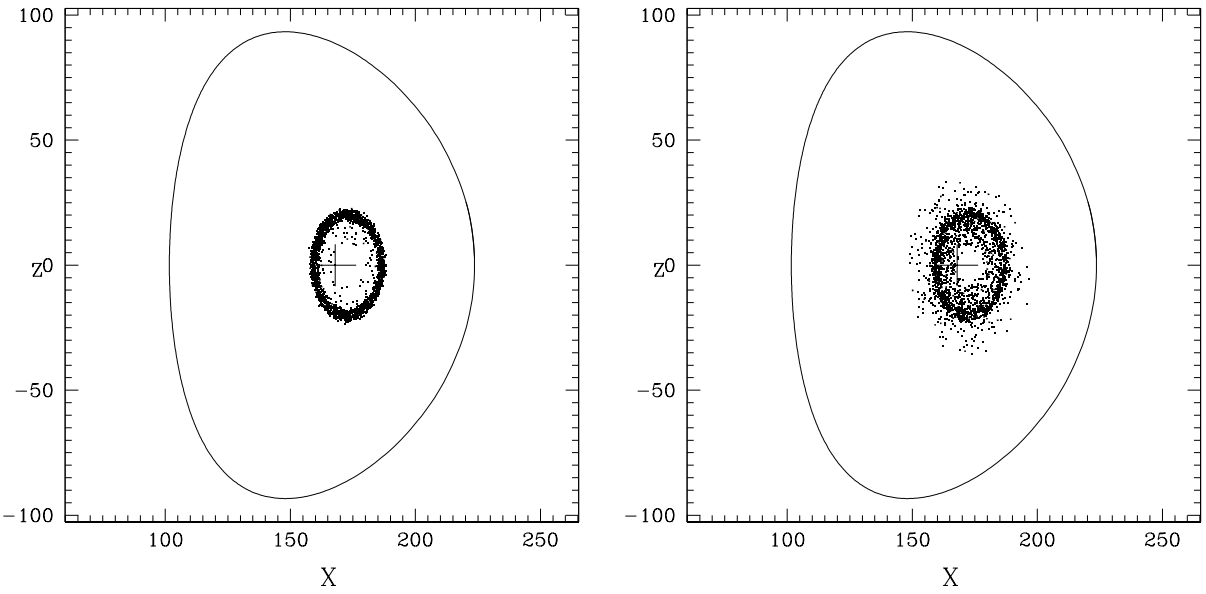

FIG. 6: Particle distribution after 7 *msec*, all launched at the outer midplane with pitch $\lambda = 0.6$ with random toroidal angle in the presence of the full spectrumn of modes, but with no collisions. Amplitudes of $dB/B \simeq 1.2 \times 10^{-4}$, (a), and $dB/B \simeq 1.6 \times 10^{-4}$, (b)

variation shown in Fig. 5, showing no noticable effect in this case. With a small number of large amplitude modes frequency sweeping can be important, but in the present case it is the induced stochasticity that drives profile change, and this is not strongly affected by mode sweeping.

To examine the final steady state of the beam profile in the presence of the modes, we include the slowing down operator, and each time a particle drops in energy below 20 Kev we replace it using a list of particles provided by TRANSP giving the beam injection. The injected beam profile is not like the final distribution shown in Fig. 3, it has a very different energy distribution. This operation results in a total replacement of the beam population every 10 *msec*. Shown in Fig. 7 is the modification of the beam profile under continuous action of the mode spectrum. Clearly a steady state distribution is obtained in approximately 50 *msec*. Note that the number of particles in the simulation is constant. The relatively small increase in density at large radius compared to the significant decrease on axis reflects the much larger volume at large radius.

Note that the mode amplitudes observed in the experiment reflect the values present after the beam profile has been flattened. It is very possible that before the beam is flattened the

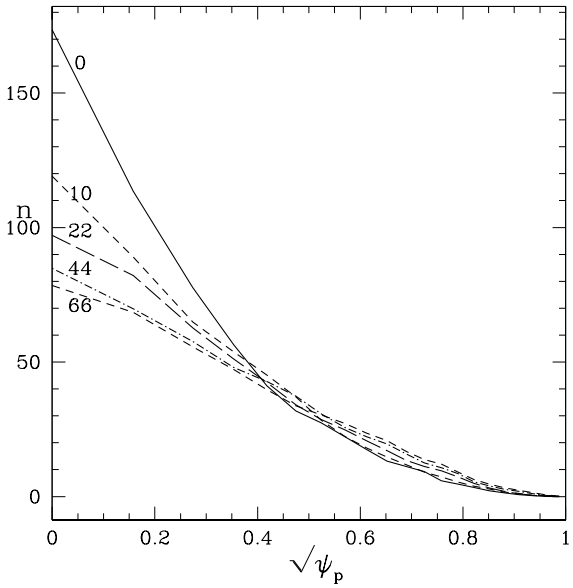

FIG. 7:

modes are more strongly driven to a larger amplitude, and that the flattening occurs in a time much shorter than 50 *msec*.

IV. CONCLUSION

In conclusion, we find that the modification of the beam profile in DIII-D from that predicted by TRANSP can be explained by the effect of the spectrum of low amplitude modes observed to be present in the discharge. Previous simulations failed because of neglect of the associated electric potential, important at frequencies high enough so that $\omega/\omega_0 \sim \rho/R$. The transport possesses a stochastic threshold, so it is very sensitive to small changes in mode content and amplitude. The fact that a sufficient number of perturbations can lead to stochastic transport in a Hamiltonian system is of course not new, it has been known since the proof of the KAM theorem and demonstrations with many models, and has also explicitely been demonstrated for TAE modes[25, 26]. The surprising result of these simulations is that even for the low amplitude modes present in the experiment the phase space of the trajectories is found to be stochastic, allowing slow but large scale modification of the distribution.

Acknowledgement

This work was partially supported by the U.S. Department of Energy Grants DE-AC02-09CH11466, SC-6903402 and DE-FC02-04ER54698. The authors acknowledge useful discussions with Y. Kolesnichenko, Y. Yakovenko and R. E. Waltz.

---

[1] W. W. Heidbrink, *Phys. Plasmas* **15**, 055501 (2008), and references therein.

[2] A. Fasoli, C. Gormenzano, H. L. Berk, B. Breizman, S. Briguglio, D. S. Darrow, N. Gorelenkov, W. W. Heidbrink, S. V. Konovalov, R.Nazikian, J. Notordaeme, S. Sharapov, K. Shinahara, D. Testa, K. Tobita, Y. Todo, G. Vlad, and F. Zonca, *Nucl. Fusion* **47** S264. (2007)

[3] M. A. Van Zeeland, G. J. Kramer, M. E. Austin, R. L. Boivin, W. W. Heidbrink, M. A. Makowski, G. R. McKee, R. Nazikian, W. M. Solomon, and G. Wang *Phys. Rev Lett.* **97**, 135001 (2006).

[4] M. A. Van Zeeland, M. E. Austin, N. N. Gorelenkov, W. W. Heidbrink, G. J. Kramer, M. A. Makowski, G. R. McKee, R. Nazikian, E. Ruskov, and A. D. Turnbull *Phys. Plasmas* **14**, 056102 (2007).

[5] M. A. Van Zeeland, W.W. Heidbrink, R. Nazikian, M. E. Austin, C. Z. Cheng, M. S. Chu, N. Gorelenkov, C. T. Holcomb, A. W. Hyatt, G. Kramer, J. Lohr, G. R. McKee, C. C. Petty, R. Practer, W. M. Solomon and D. A. Spong *Nucl. Fusion* **49**, 065003 (2009).

[6] W. W. Heidbrink, N. N. Gorelenkov, Y. Luo, M. A. Van Zeeland, R. B. White, M. E. Austin, K. H. Burrell, G. J. Kramer, M. A. Makowski, G. R. McKee, R. Nazikian, and the DIII-D team *Phys. Rev Lett.* **99** 245002 (2007)

[7] W.W. Heidbrink, M. A. Van Zeeland, M. E. Austin, K. H. Burrell, N. Gorelenkov, G. Kramer, Y. Luo, M. A. Makowski, G. R. McKee, C. Muscatello, R. Nazikian, E. Ruskov, W. M. Solomon, R. B. White, and Y. Zhu , *Nucl Fusion* **48**, 084001 (2008).

[8] Y. Luo, W. W. Heidbrink, E. Ruskov, K. H. Burrell, and W. M. Solomon, *Phys. Plasmas* **14**, 112503 (2007).

[9] Alexei Pankin, Douglas McCune, Robert Andre, Glenn Bateman, and Arnold Kritz, *Comp. Phys. Comm.* **159**, 157 (2004).

[10] R. B. White, M.S. Chance, *Phys. Fluids* **27**, 2455 (1984).

[11] R. B. White, R. J. Goldston, K. McGuire, A. H. Boozer, D. A. Monticello, and W. Park *Phys. Fluids* **26**, 2958 (1983).

[12] S. J. Zweben, D. S. Darrow, E. D. Fredrickson, G. Taylor, S. von Goeler, and R. B. White, *Nucl. Fusion* **39**, 1097 (1999).

[13] E. M. Carolipio, W. W. Heidbrink, C. B. Forest, and R. B. White, *Nucl. Fusion* **42** 853 (2002).

[14] G. Fiskel, B. Hudson, D.J. Den Hartog, R.M. Magee, R. O'Connell, S.C. Prager *Phys. Rev. Lett.* **95** *125001 (2005)* ,Y. Todo, H. L. Berk, and B. N. Breizman *Phys. Plasmas* **10** 2888 (2003)

[15] M. Garcia-Munoz, P. Martin, H. Fahrbach, M. Gobbin, S.Gunter, M. Maraschek, L. Marrelli, H. Zohm, and the ASDEX Upgrade Team *Nuc. Fus* **47** L10 (2007).

[16] D. J. Sigmar, C. T. Hsu, R. White, and C. Z. Cheng, *Phys Fluids B* **4** 1506 (1992).

[17] L. C. Appel, H. L. Berk, D. Borba et al., *Nucl. Fusion* **35** 1697 (1995)

[18] Y. Todo and T. Sato, *Phys. Plasmas* **5** 1321 (1998).

[19] J. Candy, H. L. Berk, B. N. Breizman, and F. Porcelli, *Phys. Plasmas* **6** 1822 (1999).

[20] E. M. Carolipio, W. W. Heidbrink, C. Z. Cheng, M. S. Chu, G. Y. Fu, D. A. Spong, A. D. Turnbull, and R. B. White *Phys. Plasmas* **8** 3391 (2001).

[21] Y. Todo, H. L. Berk, B. N. Breizman, et al., *Phys. Plasmas* **10** 2888 (2003).

[22] S. D. Pinches, V. G. Kiptily, S. E. Sharapov, D. S. Darrow,L. G. Eriksson, H. U. Fahrbach, M GarciMunoz, M. Reich, E. Strumberger, A. Werner, ASDEX Upgrade Team, JET-EFDA contributors, *Nucl. Fusion* **46** S904 (2006).

[23] R. B. White, N. Gorelenkov, W. W. Heidbrink, and M.A. Van Zeeland *Plasma Physics and Controlled Fusion*, to be published.

[24] R. B. White, *The Theory of Toroidally Confined Plasma* Imperial College Press, (2005).

[25] Contributed Papers, Fifth IAEA Technical Committee Meeting on Alha Particles in Fusion Research, edited by Jacquinot, Keen and Sadler, (JET Joint Undertaking, 1997), see discussion on page 74 by Berk et al.

[26] H. L. Berk, B.N. Breizman, J. Fitzpatrick and H.V. Wong, Nucl. Fusion **35**, 1661 (1995).

The Princeton Plasma Physics Laboratory is operated
by Princeton University under contract
with the U.S. Department of Energy.

Information Services
Princeton Plasma Physics Laboratory
P.O. Box 451
Princeton, NJ 08543

Phone: 609-243-2245
Fax: 609-243-2751
e-mail: pppl_info@pppl.gov
Internet Address: http://www.pppl.gov